

Dynamical polarization of graphene under strain

F. M. D. Pellegrino,^{1,2,3,4} G. G. N. Angilella,^{1,2,3,5,4} and R. Pucci^{1,2}

¹*Dipartimento di Fisica e Astronomia, Università di Catania,
Via S. Sofia, 64, I-95123 Catania, Italy*

²*CNISM, UdR Catania, I-95123 Catania, Italy*

³*Scuola Superiore di Catania, Università di Catania,
Via S. Nullo, 5/i, I-95123 Catania, Italy*

⁴*CNR-IMM, Z.I. VIII Strada 5, I-95121 Catania, Italy*

⁵*INFN, Sez. Catania, I-95123 Catania, Italy*

(Dated: October 17, 2018)

We study the dependence of the plasmon dispersion relation of graphene on applied uniaxial strain. Besides electron correlation at the RPA level, we also include local field effects specific for the honeycomb lattice. As a consequence of the two-band character of the electronic band structure, we find two distinct plasmon branches. We recover the square-root behavior of the low-energy branch, and find a nonmonotonic dependence of the strain-induced modification of its stiffness, as a function of the wavevector orientation with respect to applied strain.

PACS numbers: 73.20.Mf, 62.20.-x, 81.05.ue

I. INTRODUCTION

Graphene is a two-dimensional single layer of carbon atoms, and can be thought therefore as the building block of several sp^2 -bonded carbon allotropes, ranging from three-dimensional graphite, to one-dimensional nanotubes, to zero-dimensional fullerenes. Its recent experimental fabrication in the laboratory¹ has triggered an enormous outburst of both experimental and theoretical research. This is justified by the peculiar electronic and structural properties of graphene^{2,3}, largely due to its reduced dimensionality, as well as to correlation effects. In particular, its linear quasiparticle dispersion relation is analogous to that of relativistic massless particles, obeying Dirac-Weyl equation, thus enabling to study quantum relativistic effects in a condensed matter system^{4,5}.

Most of the unusual electronic properties of graphene are encoded in the electron polarizability, which has been studied within the Dirac cone approximation at zero⁶ and finite temperature⁷ for pristine graphene, as well as for doped graphene^{8,9}. These results have been recently extended beyond the Dirac cone approximation¹⁰. The effect of spin-orbit interaction in the electronic collective excitations of a graphene layer with or without doping has also been considered in Ref. 11.

Here, we will be concerned on the dynamical polarization of graphene within the full Brillouin zone of the honeycomb lattice. While electron correlations will be treated at the RPA level, we will explicitly include local field effects (LFE)¹², which are characteristic of the lattice structure of graphene. The importance of LFE have been shown to be more important in graphene than in bulk semiconductors, in connection with the static dielectric properties of graphene¹³. By discussing the singularities of the polarizability, we will be able to identify the collective modes of the correlated electron liquid. We will be mainly interested in the plasmon modes, which dominate the long wavelength charge density fluctua-

tions. The role of electron-plasmon interaction in renormalizing the (especially low-energy) quasiparticle dispersion relation has been emphasized^{14,15}, and plasmons in graphene are potentially interesting for applications in nanophotonics¹⁶.

Specifically, we will be interested in the dependence of the plasmon modes on applied uniaxial strain. This will enable to investigate the interplay between electronic and structural properties of graphene. It has been even suggested that nanodevices based on graphene could be engineered on the basis of the expected strain-induced modifications of the deformed graphene sheet (origami electronics)¹⁷. Indeed, graphene is also characterized by quite remarkable mechanical properties. Despite its quasi-two-dimensional character, it displays an exceptional tensile strength and stiffness¹⁸. In particular, recent *ab initio* calculations¹⁹⁻²² as well as experiments²³ have demonstrated that graphene can sustain elastic deformations as large as 20%. The possibility of a strain-induced semimetal-to-semiconductor transition, with the opening of a gap, has been therefore studied²⁴⁻²⁷. It turns out that this critically depends on the direction of applied strain, as is also confirmed by studies of the strain effect on the optical conductivity of graphene²⁸⁻³⁰.

The paper is organized as follows. In Sec. II we present our model, based on a tight-binding description of the graphene electronic band structure. We will then derive the electronic polarization at RPA level, and explicitly include local field effects. We will then derive and discuss the various branches of the plasmon modes along a symmetry contour of the first Brillouin zone, both numerically and analytically, in the limit of small wavevectors. The effect of applied uniaxial strain will then be discussed in Sec. III. Summary and concluding remarks will be given in Sec. IV.

II. MODEL

A. Tight-binding approximation

At the tight-binding level of approximation, the Hamiltonian for the graphene honeycomb lattice can be conveniently written as

$$H = \sum_{\mathbf{R}, \ell} t_\ell a^\dagger(\mathbf{R}) b(\mathbf{R} + \boldsymbol{\delta}_\ell) + \text{H.c.}, \quad (1)$$

where $a^\dagger(\mathbf{R})$ is a creation operator on the position \mathbf{R} of the A sublattice, $b(\mathbf{R} + \boldsymbol{\delta}_\ell)$ is a destruction operator on a nearest neighbor (NN) site $\mathbf{R} + \boldsymbol{\delta}_\ell$, belonging to the B sublattice, and $\boldsymbol{\delta}_\ell$ are vectors connecting NN sites on different sublattices, $\boldsymbol{\delta}_1 = a(1, \sqrt{3})/2$, $\boldsymbol{\delta}_2 = a(1, -\sqrt{3})/2$, $\boldsymbol{\delta}_3 = a(-1, 0)$, with $a = 1.42 \text{ \AA}$, the equilibrium C-C distance in a graphene sheet². In Eq. (1), $t_\ell \equiv t(\boldsymbol{\delta}_\ell)$, $\ell = 1, 2, 3$, is the hopping parameter between two NN sites. In the absence of strain they reduce to a single constant, $t_\ell \equiv t_0$, with $t_0 = -2.8 \text{ eV}$ (Ref. 31).

The dispersion relation of the valence ($\lambda = 1$) and conduction bands ($\lambda = 2$) are the solutions $E_{\mathbf{k}\lambda}$ of the generalized eigenvalue problem

$$H_{\mathbf{k}} \mathbf{u}_{\mathbf{k}\lambda} = E_{\mathbf{k}\lambda} S_{\mathbf{k}} \mathbf{u}_{\mathbf{k}\lambda}, \quad (2)$$

where

$$H_{\mathbf{k}} = \begin{pmatrix} 0 & f_{\mathbf{k}} \\ f_{\mathbf{k}}^* & 0 \end{pmatrix}, \quad (3a)$$

$$S_{\mathbf{k}} = \begin{pmatrix} 1 & g_{\mathbf{k}} \\ g_{\mathbf{k}}^* & 1 \end{pmatrix}, \quad (3b)$$

and $\gamma_{\mathbf{k}} = \sum_{\ell=1}^3 e^{i\mathbf{k}\cdot\boldsymbol{\delta}_\ell}$, $f_{\mathbf{k}} = \sum_{\ell=1}^3 t_\ell e^{i\mathbf{k}\cdot\boldsymbol{\delta}_\ell}$, $g_{\mathbf{k}} = \sum_{\ell=1}^3 s_\ell e^{i\mathbf{k}\cdot\boldsymbol{\delta}_\ell}$ are the usual (complex) structure factor, NN hopping, and overlap functions in momentum space, respectively. The hopping parameters t_ℓ and overlap parameters s_ℓ can be expressed in terms of appropriate pseudoatomic wave functions, which we here take to be normalized Gaussian, with standard deviation σ_g ^{28,32}. One finds

$$E_{\mathbf{k}\lambda} = \frac{-F_{\mathbf{k}} \mp \sqrt{F_{\mathbf{k}}^2 + 4G_{\mathbf{k}}|f_{\mathbf{k}}|^2}}{2G_{\mathbf{k}}}, \quad (4)$$

where the minus (plus) sign refers to the valence (conduction) band, and $F_{\mathbf{k}} = g_{\mathbf{k}} f_{\mathbf{k}}^* + g_{\mathbf{k}}^* f_{\mathbf{k}}$ and $G_{\mathbf{k}} = 1 - |g_{\mathbf{k}}|^2$.

In the following, we shall also use the abbreviation $\xi_{\mathbf{k}\lambda} = E_{\mathbf{k}\lambda} - \mu$, and denote $\bar{\lambda} = 2$ for $\lambda = 1$, and $\bar{\lambda} = 1$ for $\lambda = 2$. Moreover, we also set $\boldsymbol{\delta}_A = \boldsymbol{\delta}_1 + \boldsymbol{\delta}_2 + \boldsymbol{\delta}_3 = \mathbf{0}$, and $\boldsymbol{\delta}_B = \boldsymbol{\delta}_3$.

A small, albeit nonzero, value of the NN overlap $g_{\mathbf{k}}$ has the advantage of endowing valence and conduction bands with the observed asymmetry. However, since $g_{\mathbf{k}} \approx 0.07\gamma_{\mathbf{k}} \ll 1$ (also under strain, within the range considered below, in Sec. III), we can safely retain only linear corrections to the band dispersions, $E_{\mathbf{k}\lambda} = \mp|f_{\mathbf{k}}| - F_{\mathbf{k}} + \mathcal{O}(g_{\mathbf{k}}^2)$, and neglect them altogether in the eigenvectors $\mathbf{u}_{\mathbf{k}\lambda}$.

Our tight-binding approximation is completed by an appropriate choice of the Bloch wavefunctions. As in Ref. 32, we shall use $\psi_{\mathbf{k}\lambda} = N^{-1/2} \sum_j \phi(\mathbf{r} - \mathbf{R}_j^\lambda) e^{i\mathbf{k}\cdot\mathbf{R}_j^\lambda}$, where $\phi(\mathbf{r})$ is a Gaussian pseudoatomic orbital, and \mathbf{R}_j^λ are vectors of the $\lambda = A, B$ sublattices.

We can anticipate, at this stage, that some of the findings of the present study would not be obtained within the cone approximation. In particular, the tight-binding approximation allows to include important features of the electronic band dispersion, such as a finite bandwidth and the occurrence of Van Hove singularities. These features will play an essential role in deriving some of the characteristics of the plasmon dispersion, which is the main goal of the present work.

B. Local field effects on the electron polarization

Within linear response theory, plasmon modes can be described as poles of the density-density correlation function, *i.e.* the polarization. The random phase approximation (RPA) is then the simplest, infinite order, diagrammatic procedure to include electron correlations in the dielectric screening giving rise to the polarization³³. Besides electron-electron correlations, another source of \mathbf{k} -space dependence of the dielectric function is provided by local field effects (LFE)³⁴. This is due to the generally atomic consistence of matter and, in the case of solids, to the periodicity of the crystalline lattice. An account of the LFE on the dielectric function of crystalline solids dates back at least to the original paper of Adler¹² (see also Refs. 35,36), and is generalized below to the case of graphene, including both valence and conduction bands.

We start by considering the polarization, which for a noninteracting system at finite temperature T reads

$$\Pi^0(\mathbf{x}, \mathbf{x}', i\omega_m) = \hbar^{-1} (\beta\hbar)^{-1} \sum_{i\omega_n} \sum_{\mathbf{k}\lambda} \sum_{\mathbf{k}'\lambda'} \psi_{\mathbf{k}\lambda}^*(\mathbf{x}') \mathcal{G}_\lambda^0(\mathbf{k}, i\omega_n) \psi_{\mathbf{k}\lambda}(\mathbf{x}) \psi_{\mathbf{k}'\lambda'}^*(\mathbf{x}) \mathcal{G}_{\lambda'}^0(\mathbf{k}', i\omega_n + i\omega_m) \psi_{\mathbf{k}'\lambda'}(\mathbf{x}'), \quad (5)$$

where $\mathcal{G}_\lambda^0(\mathbf{k}, i\omega_n) = (i\omega_n - \xi_{\mathbf{k}\lambda}/\hbar)^{-1}$ is the Green's function for the noninteracting system, and $\hbar\omega_n = (2n+1)\pi k_B T$ [$\hbar\omega_m = 2m\pi k_B T$] denote the fermionic [bosonic] Matsubara frequencies at temperature T , with \hbar Planck's constant and k_B Boltzmann's constant. Fourier transforming into momentum space, and performing the summation over the

Matsubara frequencies, one finds

$$\Pi^0(\mathbf{q}+\mathbf{G}, -\mathbf{q}'-\mathbf{G}', i\omega_m) = (2\pi)^2 A_c^{-1} \delta(\mathbf{q}-\mathbf{q}') \frac{1}{N} \sum_{\mathbf{k}\lambda\lambda'} T_{\mathbf{k}\lambda, \mathbf{k}-\mathbf{q}\lambda'}(i\omega_m) \langle \mathbf{k}-\mathbf{q}\lambda' | e^{-i(\mathbf{q}+\mathbf{G})\cdot\hat{\mathbf{r}}} | \mathbf{k}\lambda \rangle \langle \mathbf{k}\lambda | e^{i(\mathbf{q}+\mathbf{G})\cdot\hat{\mathbf{r}}} | \mathbf{k}-\mathbf{q}\lambda' \rangle, \quad (6)$$

where

$$T_{\mathbf{k}\lambda, \mathbf{k}-\mathbf{q}\lambda'}(i\omega_m) = \frac{n_F(\xi_{\mathbf{k}-\mathbf{q}\lambda'}) - n_F(\xi_{\mathbf{k}\lambda})}{i\hbar\omega_m + \xi_{\mathbf{k}-\mathbf{q}\lambda'} - \xi_{\mathbf{k}\lambda}}. \quad (7)$$

Here, $n_F(\omega)$ is the Fermi function, $A_c = 3\sqrt{3}a^2/2$ is the area of the Wigner-Seitz cell, \mathbf{q}, \mathbf{q}' belong to the first Brillouin zone (1BZ), \mathbf{G}, \mathbf{G}' are vectors of the reciprocal lattice, and LFE are embedded in the Adler's weights¹²

$$\begin{aligned} & \langle \mathbf{k}-\mathbf{q}\lambda' | e^{-i(\mathbf{q}+\mathbf{G})\cdot\hat{\mathbf{r}}} | \mathbf{k}\lambda \rangle \\ &= \int d^2\mathbf{x} e^{-i(\mathbf{q}+\mathbf{G})\cdot\mathbf{x}} \psi_{\mathbf{k}\lambda}(\mathbf{x}) \psi_{\mathbf{k}-\mathbf{q}\lambda'}^*(\mathbf{x}) \\ &\simeq \frac{1}{2} \left[(-1)^{\lambda-\lambda'} + e^{i(\theta_{\mathbf{k}-\mathbf{q}}-\theta_{\mathbf{k}})-i\mathbf{G}\cdot\delta_3} \right] e^{-\sigma_g^2 |\mathbf{q}+\mathbf{G}|^2/4}, \quad (8) \end{aligned}$$

where in the last line only the onsite overlap between pairs of pseudoatomic orbitals, centered on either sublattices, has been retained, on account of their localized character, we have retained only the lowest (zeroth) order contributions in the overlap function $g_{\mathbf{k}}$, and $e^{i\theta_{\mathbf{k}}} = -f_{\mathbf{k}}/|f_{\mathbf{k}}|$. Using a more compact notation, one may also write

$$\begin{aligned} \Pi^0(\mathbf{q}+\mathbf{G}, -\mathbf{q}'-\mathbf{G}', i\omega_m) &= (2\pi)^2 A_c^{-1} \delta(\mathbf{q}-\mathbf{q}') \\ &\times \sum_{\alpha\beta} \rho_{\mathbf{q}\alpha}(\mathbf{G}) Q_{\alpha\beta}^0(\mathbf{q}, i\omega_m) \rho_{\mathbf{q}\beta}^*(\mathbf{G}'), \quad (9) \end{aligned}$$

where

$$\begin{aligned} Q_{\alpha\beta}^0(\mathbf{q}, i\omega_m) &= \frac{1}{N} \sum_{\mathbf{k}\lambda\lambda'} u_{\mathbf{k}\lambda}^\alpha u_{\mathbf{k}\lambda}^{\beta*} u_{\mathbf{k}-\mathbf{q}\lambda'}^{\alpha*} u_{\mathbf{k}-\mathbf{q}\lambda'}^\beta \\ &\times T_{\mathbf{k}\lambda, \mathbf{k}-\mathbf{q}\lambda'}(i\omega_m), \quad (10) \end{aligned}$$

with $u_{\mathbf{k}\lambda}^\alpha$ the components of $\mathbf{u}_{\mathbf{k}\lambda}$ ($\alpha = 1, 2$), and

$$\rho_{\mathbf{q}\alpha}(\mathbf{G}) = \exp(-i\mathbf{G}\cdot\delta_\alpha - \sigma_g^2 |\mathbf{q}+\mathbf{G}|^2/4) \quad (11)$$

are the LFE weights. The continuum limit is recovered when $\mathbf{G} = \mathbf{G}' = 0$.

Many-body correlations are then included within RPA, yielding a renormalized polarization

$$\begin{aligned} \Pi(\mathbf{q}+\mathbf{G}, -\mathbf{q}'-\mathbf{G}', i\omega_m) &= (2\pi)^2 A_c^{-1} \delta(\mathbf{q}-\mathbf{q}') \\ &\times \sum_{\alpha\beta} \rho_{\mathbf{q}\alpha}(\mathbf{G}) Q_{\alpha\beta}(\mathbf{q}, i\omega_m) \rho_{\mathbf{q}\beta}^*(\mathbf{G}'), \quad (12) \end{aligned}$$

where now

$$Q(\mathbf{q}, i\omega_m) = g_s Q^0(\mathbf{q}, i\omega_m) [\mathbb{1} - g_s A_c^{-1} V(\mathbf{q}) Q^0(\mathbf{q}, i\omega_m)]^{-1}, \quad (13)$$

where matrix products are being understood and $g_s = 2$ is a factor for spin degeneracy, and

$$V_{\alpha\beta}(\mathbf{q}) = \sum_{\mathbf{G}''} \rho_{\mathbf{q}\alpha}^*(\mathbf{G}'') V_0(\mathbf{q}+\mathbf{G}'') \rho_{\mathbf{q}\beta}(\mathbf{G}'') \quad (14)$$

is the renormalized Coulomb potential, $V_0(\mathbf{q}) = e^2/(2\varepsilon_0\varepsilon_r q)$, now a matrix over band indices. Here, $\varepsilon_r = (\varepsilon_{r1} + \varepsilon_{r2})/2$ denotes the average relative dielectric constants of the two media surrounding the graphene layer. These are air for suspended graphene ($\varepsilon_{r1} = \varepsilon_{r2} = \varepsilon_r = 1$). In the case of a stronger dielectric substrate, we expect therefore a softening of the correlation effects on the plasmon frequency. It is relevant to note that the renormalized potential already includes LFE.

C. Plasmons

Plasmons are defined as collective excitations of the electron liquid corresponding to poles of the retarded polarization,

$$\Pi(\mathbf{q}, \omega) \equiv \Pi(\mathbf{q}, -\mathbf{q}, i\omega_m \rightarrow \omega + i0^+), \quad (15)$$

where $\mathbf{q} \in 1\text{BZ}$. Here and in what follows we shall restrict to the case $\mathbf{G} = \mathbf{G}' = 0$. Indeed, it is apparent from the definition of $\Pi(\mathbf{q}, \omega)$ that its poles can only arise from the vanishing of $\det[\mathbb{1} - V(\mathbf{q})Q^0(\mathbf{q}, \omega)]$ in Eq. (13), which already contains LFE via the renormalized Coulomb potential, Eq. (14). We therefore define the dispersion relation $\omega_\ell(\mathbf{q})$ of the ℓ -th plasmon branch as

$$\Pi^{-1}(\mathbf{q}, \omega_\ell(\mathbf{q})) = 0. \quad (16)$$

This clearly involves vanishing of both real and imaginary parts of the inverse polarization. It will be useful to define the dispersion relation $\tilde{\omega}_\ell(\mathbf{q})$ of damped plasmons through

$$\text{Re} [\Pi^{-1}(\mathbf{q}, \tilde{\omega}_\ell(\mathbf{q}))] = 0. \quad (17)$$

Correspondingly, the inverse lifetime $\tau^{-1}(\mathbf{q}, \omega)$ of such damped plasmons is proportional to $-\text{Im} \Pi(\mathbf{q}, \omega)$, for $\omega = \tilde{\omega}_\ell(\mathbf{q})$.

Fig. 1 shows our numerical results for the plasmon dispersion relation in doped graphene ($\mu = 1$ eV) at finite temperature ($T = 3$ K) along a symmetry contour in the 1BZ, without LFE [$\mathbf{G}'' = 0$ in Eq. (14), top panel] and including LFE (bottom panel). At small wavevectors and low frequencies, one recognizes a square-root plasmon mode $\omega_1(\mathbf{q}) \sim \sqrt{q}$, typical of a 2D system³³. This is

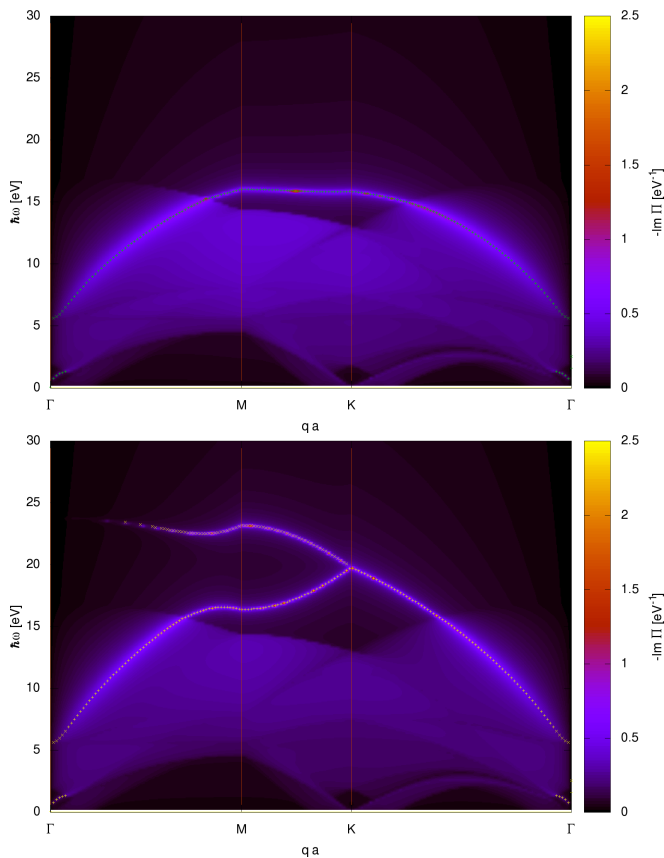


FIG. 1: (Color online) Plasmon dispersion relation for doped graphene ($\mu = 1$ eV) at finite temperature ($T = 3$ K), not including (top panel) and including (bottom panel) LFE. Results are shown along a symmetry contour in the 1BZ, with $\Gamma = (0, 0)$, $\mathbf{M} = (2\pi/3a, 0)$, and $\mathbf{K} = (2\pi/3a, 2\pi/3\sqrt{3}a)$. Frequencies ω are in eV. The shaded background is a contour plot of $-\text{Im} \Pi(\mathbf{q}, \omega)$ (arbitrary scale), while continuous lines are the dispersion relation of damped plasmons, $\tilde{\omega}_\ell(\mathbf{q})$, Eq. (17), is shown as a dotted line.

in agreement with earlier studies of the dynamical screening effects in graphene at RPA level, employing an approximate conic dispersion relation for electrons around the Dirac points^{8,9}. Such a result has been confirmed also for a tight-binding band^{10,37}, and is here generalized with the inclusion of LFE. The effect of spin-orbit interaction can be neglected, in the case of sufficiently large chemical potential¹¹, as is here the case.

The high energy (5 – 20 eV) pseudo-plasmon mode, extending throughout the whole 1BZ, is rather associated with a logarithmic singularity of the bare polarization $Q^0(\mathbf{q}, \omega)$ in Eq. (13), and therefore does not correspond to a true pole of the polarization. This collective mode can be related to an interband transition between the Van Hove singularities in the valence and conduction bands of graphene, and has been identified with a $\pi \rightarrow \pi^*$ transition^{10,38}.

At large wavevectors, specifically along the zone boundary between the \mathbf{M} and the \mathbf{K} (Dirac) points, full

inclusion of LFE determines the appearance of a second, high-frequency (20 – 25 eV), optical-like plasmon mode $\omega_2(\mathbf{q})$, weakly dispersing as $q \rightarrow 0$. Multiple plasmon modes are a generic consequence of the possibility of interband transitions, whenever several such bands are available. This is *e.g.* the case of quasi-2D quantum wells (2DQW), whose energy spectrum is characterized by quantized levels in the direction perpendicular to the plane of the well, while electrons can roam freely within the plane³³. In this case, collective modes arise as zeroes of the determinant of the dielectric function. At low temperatures, at most the two lowest subbands need to be considered. One usually obtains a longitudinal ‘acoustic’ mode associated to intrasubband coupling, and a transverse ‘optical’ mode associated to intersubband coupling³⁹. Such a situation is here paralleled by the case of graphene, the role of the two subbands of 2DQW being here played by the valence and conduction bands, touching at the Dirac points in the neutral material. It should be noticed that the plasmon mode due to interband coupling is exactly suppressed when LFE are neglected. In 2DQW, the discrete nature of the electronic subbands is due to the real-space confinement of the electron liquid in the direction perpendicular to the plane, *i.e.* to the *quasi*-2D character of the quantum well. In graphene, the origin of the two bands ultimately lies in the specific lattice structure of this material. Therefore, the high-energy, ‘optical’ plasmon mode disappears in the absence of LFE (Fig. 1, top panel), as expected whenever the lattice structure of graphene is neglected. In other words, while in the absence of LFE only scattering processes with momenta within the 1BZ are considered, LFE allow to include all scattering processes with arbitrarily low wavelengths, thereby taking into account the discrete nature of the crystalline lattice. Such a structure needs not be considered in the case of a 2DQW. Our finding of a high-energy ‘optical’ plasmon branch, as generic consequence of the two-band electronic structure of graphene, should stimulate further investigation of the electronic collective modes in graphene^{37,40}, in view of the role of electron-electron correlations in interpreting electron spectroscopy for interband transitions⁴¹.

D. Asymptotic behaviors

In certain limiting regimes, one may derive the asymptotic behavior of the polarization in close form. At low energies ($\hbar\omega \lesssim |t|$) and small wavevectors ($q \rightarrow 0$, *i.e.* $q\sigma_g \ll 1$), LFE can be neglected. The matrix product entering the definition of the polarization through Eq. (13) then reduces to

$$\begin{aligned}
 g_s A_c^{-1} V(\mathbf{q}) Q^0(\mathbf{q}, \omega) &= g_s A_c^{-1} V_0(\mathbf{q}) \sum_{\alpha\beta} Q_{\alpha\beta}^0(\mathbf{q}, \omega) \\
 &= \frac{\tilde{V}_0}{q a N} \sum_{\mathbf{k}\lambda} \delta_T(\xi_{\mathbf{k}\lambda}) \left(\frac{\mathbf{q} \cdot \nabla_{\mathbf{k}} E_{\mathbf{k}\lambda}}{\hbar\omega} \right)^2 \quad (8)
 \end{aligned}$$

where $\tilde{V}_0 = g_s(8\pi/3\sqrt{3})(a_0/a)$ Ry, a_0 being Bohr's radius, and $\delta_T(\epsilon) \equiv -\partial n_F(\epsilon)/\partial \epsilon \rightarrow \delta(\epsilon)$, as $T \rightarrow 0$. In the latter limit, the δ -function effectively restricts the integration over wavevectors along the Fermi line. Whenever the cone approximation holds (*i.e.*, for sufficiently low chemical potential and strain; see Sec. III), this can be taken as the constant-energy ellipse in Eq. (17) of Ref. 28. The \mathbf{k} -integration in Eq. (18) can then be performed analytically, and the retarded polarization, Eq. (15), then reads

$$\Pi(\mathbf{q}, \omega) \approx \frac{g_s A_c^{-1} \tilde{V}_0^{-1} \tilde{\omega}_1^2 q^2 a^2}{\hbar^2 \omega^{+2} - \hbar^2 \omega_1^2(\mathbf{q})}, \quad (19)$$

where $\omega^+ \equiv \omega + i0^+$, and

$$\hbar \tilde{\omega}_1 = \left(\frac{1}{2} \tilde{V}_0 \rho(\mu) \right)^{1/2} |\nabla_{\mathbf{q}} E_{\mathbf{q}2}/a|, \quad (20)$$

with $g_s \rho(\mu)$ the density of states (DOS) at the Fermi level. To leading order in qa , from Eq. (19) one thus obtains

$$\omega_1(\mathbf{q}) \approx \tilde{\omega}_1 \sqrt{qa} \quad (21)$$

for the acoustic-like plasmon dispersion relation. One thus recovers the square-root behavior of the plasmon dispersion relation, as is typical in 2D electron systems³³. Moreover, one recovers the dependence of the coefficient $\tilde{\omega}_1 \sim n^{1/4}$ on the carrier density n , rather than $\sim n^{1/2}$, as is the case for a parabolic dispersion relation of the quasiparticles^{9,42}. The acoustic-like plasmon mode may be related to the Drude weight⁴³, thus enabling the observation of strain effects from optical measurements⁴⁴. In the case of graphene on a dielectric substrate ($\epsilon_r > 1$), one has a reduction of $\tilde{\omega}_1$, thus a softening of the plasmon mode. From Eq. (19) one may also read off the imaginary part of the retarded polarization, which close to the 'acoustic' plasmon mode [$\omega \sim \omega_1(\mathbf{q})$] reads

$$\text{Im} \Pi(\mathbf{q}, \omega^+) \approx -\frac{\pi}{2} g_s A_c^{-1} \tilde{V}_0^{-1/2} \tilde{\omega}_1 (qa)^{3/2} \delta(\omega - \omega_1(\mathbf{q})). \quad (22)$$

We now turn to the asymptotic behavior of the second branch of the plasmonic spectrum, $\omega_2(\mathbf{q})$. We have already established that it displays an optical-like character, with $\omega_2(\mathbf{q}) \rightarrow \omega_2(0)$, as $q \rightarrow 0$. Here, $\omega_2(0)$ is greater than the distance between the top of the conduction band and the bottom of the valence band. At small wavevectors, it is useful to consider the expansions of the relevant terms in Eq. (13), which to leading order in q_i ($i = x, y$) read

$$Q_{AA}^0(\mathbf{q}, \omega) \approx Q_{AA}(0, \omega) + \sum_{ij} q_i y_{ij}(\omega) q_j, \quad (23a)$$

$$Q_{AB}^0(\mathbf{q}, \omega) \approx -Q_{AA}(0, \omega) + \sum_{ij} q_i z_{ij}(\omega) q_j, \quad (23b)$$

where $y_{ij}(\omega)$, $z_{ij}(\omega)$ are real valued functions of the frequency ω , and

$$Q_{AA}^0(0, \omega_2(0)) = \frac{1}{4N} \sum_{\mathbf{k}\lambda} \frac{n_F(\xi_{\mathbf{k}\bar{\lambda}}) - n_F(\xi_{\mathbf{k}\lambda})}{\omega_2(0) + \xi_{\mathbf{k}\bar{\lambda}} - \xi_{\mathbf{k}\lambda}}. \quad (24)$$

The asymptotically constant value of the optical-like plasmon frequency is then implicitly given by

$$1 - 4Q_{AA}^0(0, \omega_2(0)) g_s A_c^{-1} \sum_{\mathbf{G}} V(\mathbf{G}) \sin^2 \left(\frac{1}{2} \mathbf{G} \cdot \boldsymbol{\delta}_3 \right) = 0, \quad (25)$$

whereas the imaginary part of the retarded polarization, close to the second plasmon branch [$\omega \sim \omega_2(0)$], to leading order in q , reads

$$\text{Im} \Pi(\mathbf{q}, \omega^+) \approx -\pi g_s A_c^{-1} \left| \frac{1}{4N} \sum_{\mathbf{k}\lambda} \frac{n_F(\xi_{\mathbf{k}\bar{\lambda}}) - n_F(\xi_{\mathbf{k}\lambda})}{(\omega_2(0) + \xi_{\mathbf{k}\bar{\lambda}} - \xi_{\mathbf{k}\lambda})^2} \right|^{-1} \times \sum_{ijhk} q_i q_h (z_{ij} - y_{ij})(z_{hk} + y_{hk}) q_j q_k \delta(\omega - \omega_2(0)) \quad (26)$$

In particular, it follows that the spectral weight of $\text{Im} \Pi$ close to $\omega_2(0)$ decreases as $\sim q^4$, as $q \rightarrow 0$, rather than as $\sim q^{3/2}$, as is the case for the acoustic-like plasmon mode, Eq. (22). This justifies the reduced spectral weight associated with the second plasmon branch at small wavevector in Fig. 1. In the case of graphene on a dielectric substrate ($\epsilon_r > 1$), inspection of Eqs. (24) and (25) yields a reduction of $\omega_2(0)$.

III. EFFECT OF STRAIN ON THE PLASMON DISPERSION RELATION

We now turn to consider the effect of strain on the plasmon dispersion relation. As in Refs. 25,28, applied uniaxial strain can be modeled by explicitly considering the dependence on the strain tensor $\boldsymbol{\varepsilon}$ of the tight-binding parameters $t_\ell = t(\boldsymbol{\delta}_\ell)$ through the vectors $\boldsymbol{\delta}_\ell$ connecting two NN sites ($\ell = 1, 2, 3$). A linear dependence of $\boldsymbol{\delta}_\ell$ on $\boldsymbol{\varepsilon}$ is justified in the elastic limit. Such an assumption is however quite robust, due to the extreme rigidity of graphene¹⁸, and is supported by *ab initio* calculations^{19,21}.

Below, the strain tensor $\boldsymbol{\varepsilon}$ will be parametrized by a strain modulus ε , and by the angle θ between the direction of applied strain and the x axis in the lattice coordinate system. Specifically, one has $\theta = 0$ [*resp.*, $\theta = \pi/6$] for strain applied along the armchair [*resp.*, zig-zag] direction.

The main effect of applied strain on the band dispersion relation is that of shifting the location of the Dirac points $\pm \mathbf{k}_D$ from their position $\pm \mathbf{K}$ at $\varepsilon = 0$. While valence and conduction bands vanish linearly as $\mathbf{q} \rightarrow \pm \mathbf{k}_D$ for moderately low applied strain, such an approximation breaks down at a critical value of the strain modulus ε , depending on the direction θ of applied strain, when $\pm \mathbf{k}_D$ tends to either midpoint \mathbf{M}_ℓ of the 1BZ border. This has been described in terms of an electronic topological transition (ETT), since it is accompanied by a change of topology of the Fermi line²⁸.

Fig. 2 shows the dispersion relation of the plasmon branches studied in Sec. IIC, including LFE, along a

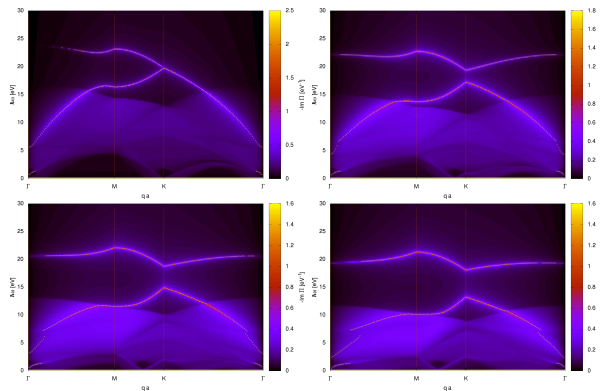


FIG. 2: (Color online) Plasmon dispersion relation for doped graphene at finite temperature ($\mu = 1$ eV, $T = 3$ K), including LFE, with strain applied along the $\theta = 0$ (armchair) direction. Strain increases (from left to right, from top to bottom) as $\varepsilon = 0, 0.075, 0.175, 0.275$.

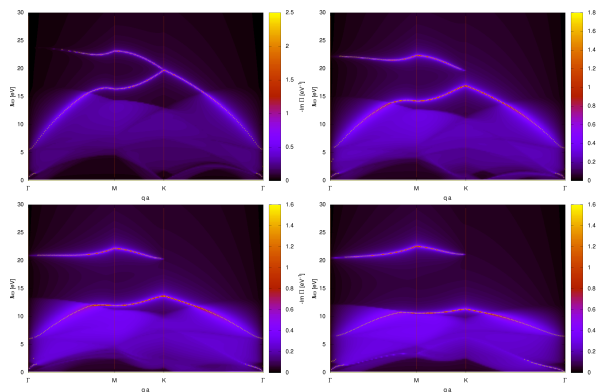


FIG. 3: (Color online) Plasmon dispersion relation for doped graphene at finite temperature ($\mu = 1$ eV, $T = 3$ K), including LFE, with strain applied along the $\theta = \pi/6$ (zig-zag) direction. Strain increases (from left to right, from top to bottom) as $\varepsilon = 0, 0.075, 0.175, 0.275$.

symmetry contour of the 1BZ, for strain applied along the armchair direction ($\theta = 0$), with increasing strain modulus ($\varepsilon = 0 - 0.275$). The low-frequency, ‘acoustic’ plasmon mode $\omega_1(\mathbf{q})$ is not qualitatively affected by the applied strain. In particular, the dominant square-root behavior is independent with respect to the opening of a gap. On the other hand, one observes an increase of spectral weight associated with the high-frequency, ‘optical’ plasmon mode $\omega_2(\mathbf{q})$ at small wavevectors. The overall flattening of the second plasmon branch over the symmetry contour under consideration can be traced back to the strain-induced shrinking of both valence and conduction bands. We also note the formation of a gap between $\omega_2(\mathbf{q})$ and the pseudo-plasmon mode corresponding to a logarithmic singularity in $Q^0(\mathbf{q}, \omega)$ at $\mathbf{q} = \mathbf{K}$.

A qualitatively similar analysis applies to the case of strain applied along the zig-zag direction ($\theta = \pi/6$,

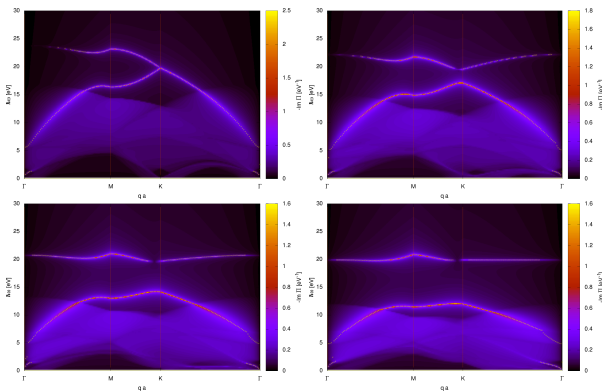


FIG. 4: (Color online) Plasmon dispersion relation for doped graphene at finite temperature ($\mu = 1$ eV, $T = 3$ K), including LFE, with strain applied along the $\theta = \pi/4$ (generic) direction. Strain increases (from left to right, from top to bottom) as $\varepsilon = 0, 0.075, 0.175, 0.275$.

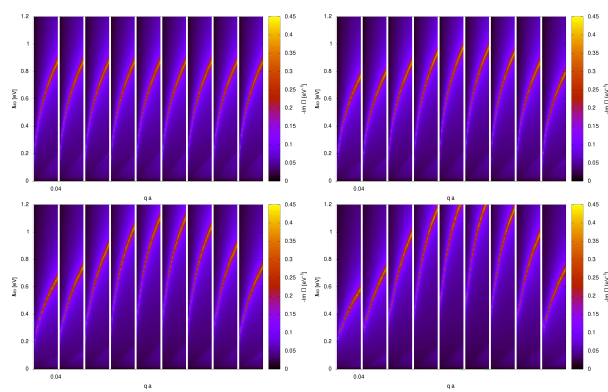


FIG. 5: (Color online) Plasmon dispersion relation for doped graphene at finite temperature ($\mu = 1$ eV, $T = 3$ K), including LFE, with strain applied along the $\theta = 0$ (armchair) direction. Strain increases (from left to right, from top to bottom) as $\varepsilon = 0, 0.075, 0.175, 0.275$. In each graph, different panels refer to $\omega_1(\mathbf{q}) = \omega_1(q, \varphi_{\mathbf{q}})$, with $\varphi_{\mathbf{q}} = 0^\circ, 20^\circ, 40^\circ, \dots, 160^\circ$.

Fig. 3), and for strain applied along a generic direction ($\theta = \pi/4$, Fig. 4), with $\omega_2(\mathbf{q})$ dispersing more weakly as the strain increases.

Finally, we turn to study the \mathbf{q} -dependence of the low-frequency, ‘acoustic’ mode $\omega_1(\mathbf{q}) \equiv \omega_1(q, \varphi_{\mathbf{q}})$ under applied strain, where $q = |\mathbf{q}|$ and $\varphi_{\mathbf{q}}$ denotes the angle between \mathbf{q} and the x axis. Fig. 5 shows then the dispersion relation of the lower plasmon branch as a function of q for several values of $\varphi_{\mathbf{q}}$, for increasing strain applied along the armchair direction ($\theta = 0$). While the overall square-root shape $\omega_1 \approx \tilde{\omega}_1 \sqrt{qa}$, Eq. (21), is maintained in all cases, one observes a stiffening of such plasmonic mode with increasing strain and a maximum of the coefficient $\tilde{\omega}_1$, Eq. (20), when $\varphi_{\mathbf{q}} - \theta \approx 90^\circ$. The same description qualitatively applies also to the cases of strain applied along the armchair ($\theta = \pi/6$), and along a generic

($\theta = \pi/4$) direction. Such a behavior can be justified analytically in the limit of no LFE (cf. Sec. IID), and corresponds to the strain dependence obtained for the optical conductivity²⁸. Indeed, from Eq. (20), one may notice that all the strain dependence is contained in the modulus square of the quasiparticle dispersion relation of the conduction band at the Fermi level, $|\nabla_{\mathbf{q}}E_{\mathbf{k}2}/a|$. One finds

$$\tilde{\omega}_1 \propto |\nabla_{\mathbf{q}}E_{\mathbf{q}2}| = \left(\frac{\cos^2(\varphi_{\mathbf{q}} - \eta)}{A^2} + \frac{\sin^2(\varphi_{\mathbf{q}} - \eta)}{B^2} \right)^{1/2}, \quad (27)$$

where A and B denote the semiaxes of the constant energy ellipse²⁸,

$$A^{-2} = \frac{1}{2}(\gamma - \sqrt{\alpha^2 + \beta^2}), \quad (28a)$$

$$B^{-2} = \frac{1}{2}(\gamma + \sqrt{\alpha^2 + \beta^2}), \quad (28b)$$

with

$$\alpha = -\frac{3}{2}a^2(t_1^2 + t_2^2 - 2t_3^2), \quad (29a)$$

$$\beta = \frac{3\sqrt{3}}{2}a^2(t_1^2 - t_2^2), \quad (29b)$$

$$\gamma = \frac{3}{2}a^2(t_1^2 + t_2^2 + t_3^2), \quad (29c)$$

and

$$\cos(2\eta) = \frac{|\alpha|}{\sqrt{\alpha^2 + \beta^2}}, \quad (30a)$$

$$\sin(2\eta) = \frac{|\alpha|}{\alpha} \frac{\beta}{\sqrt{\alpha^2 + \beta^2}}. \quad (30b)$$

It follows that $\tilde{\omega}_1$ attains its maximum values whenever $\varphi_{\mathbf{q}} - \eta = \pi/2$ (modulo π), and its minimum values when-

ever $\varphi_{\mathbf{q}} - \eta = 0$ (modulo π). It turns out that $\eta = \theta$ in the zig-zag and armchair cases (cf. Fig. 5), whereas $\eta \simeq \theta$ in the generic case.

IV. CONCLUSIONS

By studying the electronic polarization, we have derived the dispersion relation of the plasmon modes in graphene. Besides including electron-electron correlation at the RPA level, we have also considered local field effects, that are specific to the peculiar lattice structure under study. As a consequence of the two-band character of the electronic band structure of graphene, we find in general two plasmonic branches: (1) a low-energy, acoustic-like one with a square-root behavior at small wavevectors, and (2) a high-energy, optical-like mode, weakly dispersing at small wavevectors. This is generic to two-band systems, and might apply to other two-band systems as well, such as MgB_2 , and is analogous to the collective modes in two-dimensional quantum wells. We also find an intermediate energy pseudo-plasmon mode, associated with a logarithmic (*viz.* non power-law) divergence of the polarization, which can be related to an interband transition between the Van Hove singularities in the valence and conduction bands of graphene, and can be identified with a $\pi \rightarrow \pi^*$ transition. We have next studied, both analytically and numerically, the dependence of the plasmon branches on applied strain. While the square-root character of the low-energy mode at small wavevector is robust with respect to applied strain, we find a nonmonotonic stiffening as a function of the wavevector direction, the maximum steepness occurring roughly when the latter is orthogonal to the direction of applied strain. We have also studied the influence of applied strain on the high-energy, optical-like plasmon branch.

¹ K. S. Novoselov, D. Jiang, F. Schedin, T. J. Booth, V. V. Khotkevich, S. V. Morozov, and A. K. Geim, Proc. Nat. Acad. Sci. **102**, 10451 (2005).

² A. H. Castro Neto, F. Guinea, N. M. R. Peres, K. S. Novoselov, and A. K. Geim, Rev. Mod. Phys. **81**, 000109 (2009).

³ D. S. L. Abergel, V. Apalkov, J. Berashevich, K. Ziegler, and T. Chakraborty, Adv. Phys. **59**, 261 (2010).

⁴ Y. Zhang, Y. Tan, H. L. Stormer, and P. Kim, Nature **438**, 201 (2005).

⁵ C. Berger, Z. Song, X. Li, X. Wu, N. Brown, C. Naud, D. Mayou, T. Li, J. Hass, A. N. Marchenkov, et al., Science **312**, 1191 (2006).

⁶ J. González, F. Guinea, and M. A. H. Vozmediano, Phys. Rev. B **59**, R2474 (1999).

⁷ O. Vafek, Phys. Rev. Lett. **97**, 266406 (2006).

⁸ B. Wunsch, T. Stauber, F. Sols, and F. Guinea, New Journal of Physics **8**, 318 (2006), URL <http://stacks.iop.org/1367-2630/8/i=12/a=318>.

⁹ E. H. Hwang and S. Das Sarma, Phys. Rev. B **75**, 205418 (2007).

¹⁰ T. Stauber, J. Schliemann, and N. M. R. Peres, Phys. Rev. B **81**, 085409 (2010).

¹¹ X.-F. Wang and T. Chakraborty, Phys. Rev. B **75**, 033408 (2007).

¹² S. L. Adler, Phys. Rev. **126**, 413 (1962).

¹³ M. van Schilfgaarde and M. I. Katsnelson, (2010), preprint [arXiv:1006.2426v1](https://arxiv.org/abs/1006.2426v1).

¹⁴ A. Bostwick, T. Ohta, T. Seyller, K. Horn, and E. Rotenberg, Nat. Phys. **3**, 36 (2007).

¹⁵ V. W. Brar, S. Wickenburg, M. Panlasigui, C.-H. Park, T. O. Wehling, Y. Zhang, R. Decker, Ç. Girit, A. V. Balatsky, S. G. Louie, et al., Phys. Rev. Lett. **104**, 036805 (2010).

¹⁶ M. Jablan, H. Buljan, and M. Soljačić, Phys. Rev. B **80**, 245435 (2009).

- ¹⁷ V. M. Pereira and A. H. Castro Neto, Phys. Rev. Lett. **103**, 046801 (2009).
- ¹⁸ T. J. Booth, P. Blake, R. R. Nair, D. Jiang, E. W. Hill, U. Bangert, A. Bleloch, M. Gass, K. S. Novoselov, M. I. Katsnelson, et al., Nano Letters **8**, 2442 (2008).
- ¹⁹ J.-W. Jiang, J.-S. Wang, and B. Li, Phys. Rev. B **81**, 073405 (2010).
- ²⁰ S.-M. Choi, S.-H. Jhi, and Y.-W. Son, Phys. Rev. B **81**, 081407 (2010).
- ²¹ E. Cadelano, P. L. Palla, S. Giordano, and L. Colombo, Phys. Rev. Lett. **102**, 235502 (2009).
- ²² F. Liu, P. Ming, and J. Li, Phys. Rev. B **76**, 064120 (2007).
- ²³ K. S. Kim, Y. Zhao, H. Jang, S. Y. Lee, J. M. Kim, K. S. Kim, J. H. Ahn, P. Kim, J. Choi, and B. H. Hong, Nature **457**, 706 (2009).
- ²⁴ G. Cocco, E. Cadelano, and L. Colombo, Phys. Rev. B **81**, 241412 (2010).
- ²⁵ V. M. Pereira, A. H. Castro Neto, and N. M. R. Peres, Phys. Rev. B **80**, 045401 (2009), preprint [arXiv:0811.4396](https://arxiv.org/abs/0811.4396).
- ²⁶ G. Gui, J. Li, and J. Zhong, Phys. Rev. B **78**, 075435 (2008).
- ²⁷ R. M. Ribeiro, V. M. Pereira, N. M. R. Peres, P. R. Briddon, and A. H. C. Neto, New J. Phys. **11**, 115002 (2009).
- ²⁸ F. M. D. Pellegrino, G. G. N. Angilella, and R. Pucci, Phys. Rev. B **81**, 035411 (2010).
- ²⁹ F. M. D. Pellegrino, G. G. N. Angilella, and R. Pucci, High Press. Res. **29**, 569 (2009).
- ³⁰ It is relevant to add that deformed honeycomb lattices may be realized not only in strained graphene, but also in suitably designed optical lattices⁴⁵. In that context, it has been emphasized that as a function of strain, there exists a critical deformation beyond which a gap opens in the energy spectrum of both material (graphene) and optical lattices, and that Klein tunneling loses its relativistic character beyond the critical deformation, depending on the direction of applied strain.
- ³¹ S. Reich, J. Maultzsch, C. Thomsen, and P. Ordejón, Phys. Rev. B **66**, 035412 (2002).
- ³² F. M. D. Pellegrino, G. G. N. Angilella, and R. Pucci, Phys. Rev. B **80**, 094203 (2009).
- ³³ G. Giuliani and G. Vignale, *Quantum Theory of the Electron Liquid* (Cambridge University Press, Cambridge, 2005).
- ³⁴ W. Schattke, in *Encyclopedia of Condensed Matter Physics*, edited by F. Bassani, G. L. Liedl, and P. Wyder (Elsevier, Amsterdam, 2005), vol. 1, p. 145.
- ³⁵ W. Hanke and L. J. Sham, Phys. Rev. Lett. **33**, 582 (1974).
- ³⁶ W. Hanke and L. J. Sham, Phys. Rev. B **12**, 4501 (1975).
- ³⁷ A. Hill, S. A. Mikhailov, and K. Ziegler, EPL (Europhysics Letters) **87**, 27005 (2009), URL <http://stacks.iop.org/0295-5075/87/i=2/a=27005>.
- ³⁸ M. H. Gass, U. Bangert, A. L. Bleloch, P. Wang, R. R. Nair, and A. K. Geim, Nature Nanotech. **3**, 676 (2008).
- ³⁹ C. A. Ullrich and G. Vignale, Phys. Rev. B **65**, 245102 (2002).
- ⁴⁰ T. Eberlein, U. Bangert, R. R. Nair, R. Jones, M. Gass, A. L. Bleloch, K. S. Novoselov, A. Geim, and P. R. Briddon, Phys. Rev. B **77**, 233406 (2008).
- ⁴¹ M. Polini, R. Asgari, G. Borghi, Y. Barlas, T. Pereg-Barnea, and A. H. MacDonald, Phys. Rev. B **77**, 081411 (2008).
- ⁴² S. Das Sarma and E. H. Hwang, Phys. Rev. Lett. **102**, 206412 (2009).
- ⁴³ M. Polini, A. H. MacDonald, and G. Vignale,, ... (2009), preprint [arXiv:0901.4528v1](https://arxiv.org/abs/0901.4528v1).
- ⁴⁴ F. M. D. Pellegrino, G. G. N. Angilella, and R. Pucci, High Press. Res. ..., ... (2010).
- ⁴⁵ O. Bahat-Treidel, O. Peleg, M. Grobman, N. Shapira, M. Segev, and T. Pereg-Barnea, Phys. Rev. Lett. **104**, 063901 (2010).